



An in-depth investigation of physico-electro chemical properties of NiCo_2S_4 nano composites for high-performance supercapacitor applications

A. Premkumar¹ · B. Sridevi¹ · K. S. Mohan²

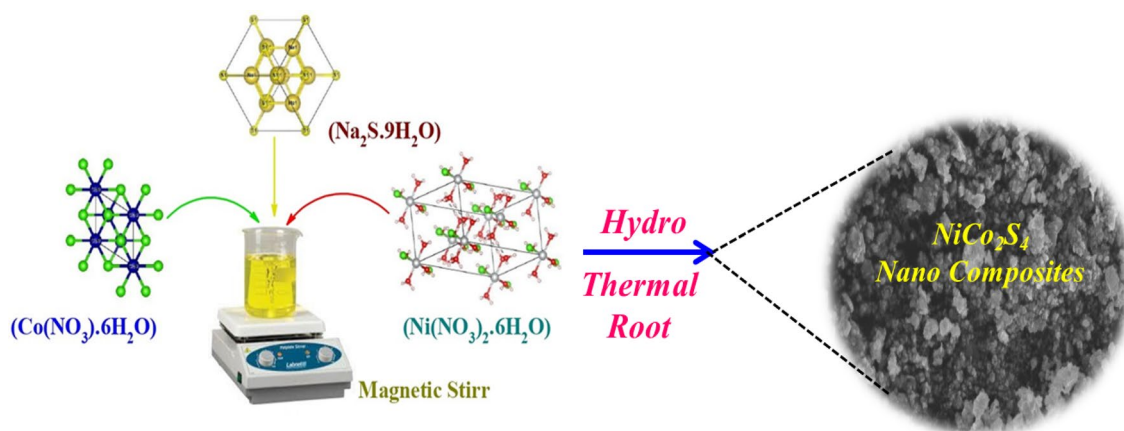
Received: 9 April 2024 / Accepted: 29 June 2024

© The Author(s), under exclusive licence to Springer Nature B.V. 2024

Abstract

In recent years, spinel-type NiCo_2S_4 has garnered considerable attention as a promising material for supercapacitors due to its high theoretical capacitance and cost-effectiveness, typically synthesised via the hydrothermal method. However, its application as a standalone electrode material is hindered by limited cycling stability. To overcome this challenge and enhance its electrochemical performance, researchers have turned to developing composite materials incorporating NiCo_2S_4 . In our pursuit of improving electrode properties for efficient supercapacitors, synthesising composites of NiCo_2S_4 typically involves combining nickel (Ni), cobalt (Co), and sulphur (S) precursors with other materials to form a nanostructured composite. Specifically, we employed this composite in an asymmetric supercapacitor (ASC) with a KOH electrolyte, utilising synthesised graphene oxide as the anode material. The resulting ASC exhibited remarkable performance metrics, boasting a high specific capacity of 1450 Fg^{-1} at 0.25 Ag^{-1} , excellent capacitance retention of 89.03% after 10,000 cycles, and an impressive energy density of 76.47 Wh kg^{-1} at 201.01 W kg^{-1} , alongside outstanding flexibility. Our study highlights the promising potential of porous NiCo_2S_4 composite electrodes in advancing the field of supercapacitors.

Graphical Abstract



Keywords Transition metal sulfide · Electrocatalyst · Energy storage and catalyst synthesis

1 Introduction

Supercapacitors, also known as electrochemical capacitors or ultracapacitors, bridge the gap between traditional capacitors and batteries, offering unique advantages such as

Extended author information available on the last page of the article

high-power density, rapid charge and discharge rates, long cycle life, and excellent temperature performance. They store energy through charge separation at the electrode–electrolyte interface, often utilizing high-surface-area electrodes and electrochemical double-layer capacitance or pseudo-capacitance mechanisms. Supercapacitors have the potential to significantly impact daily lives [1, 2] in various ways. They excel in power delivery [3–5], enabling rapid energy transfer and peak power handling in applications like electric vehicles, hybrid energy systems, and grid stabilization. Additionally, supercapacitors play a crucial role in energy harvesting from renewable sources, quickly storing excess energy during high-production periods for later use, thereby enhancing overall energy efficiency and reliability. These nanomaterials exhibit various forms, including nanosheet arrays, nanotubes [6], nanorods [7], urchins [8], hollow spheres [9], nano-buds [10], and flowers [11]. Notably, ternary sulfides like nickel–cobalt sulfides exhibit distinctive physical, chemical, and electrochemical properties that contribute to their superior performance. Supercapacitors enhance renewable energy system efficiency and grid integration. In portable electronics, their high-power density and fast charging suit rapid charging needs for smartphones, wearables, etc. Industries use them for frequent cycling and high-power demands, seen in transportation (electric buses), aerospace (regenerative braking), and telecommunications (data center backup). Supercapacitors aid energy efficiency by capturing and utilizing excess energy, reducing waste [12]. With low self-discharge rates and minimal maintenance needs, they promote sustainability over traditional storage methods. Supercapacitor energy storage devices offer high-power output, long cycle life, and fast charging, making them essential for quick energy delivery and storage. Their adoption enhances energy efficiency, sustainability, and technological advancement [13]. Research in sustainable electrochemical energy conversion focuses on environmentally friendly methods for energy generation, conversion, and storage. This includes improving fuel cells and electrolyzers for efficient energy conversion and developing advanced materials and designs for batteries and supercapacitors to enhance energy density, cycle life, and safety. Integration of renewable energy sources like solar and wind power enables efficient energy utilization by storing excess energy for later use. Overall, sustainable electrochemical energy conversion and storage methods are pivotal in transitioning towards a cleaner and more efficient energy future through interdisciplinary research and innovation. Researchers aim to develop devices meeting high-power output, long lifetime, and short charging time demands across fields like energy storage, portable electronics, electric vehicles, and renewable energy integration. Focus areas include improving power and energy density in storage systems, exploring advanced materials, optimizing cell designs, and enhancing cycle life for

prolonged durability. Ternary sulfide nanocomposites, such as NiCo_2S_4 , display unique physical, chemical, and electrochemical characteristics. These properties encompass high specific capacitance, exceptional electrochemical stability, and enhanced electronic and electrical conductivity, surpassing both oxide counterparts and binary sulfides [13, 14]. Moreover, the integration of cobalt (Co) and nickel (Ni) in bimetallic sulfides elevates the redox potential and enhances electrochemical energy storage performance compared to monometallic sulfides [15]. In the pursuit of high-performance supercapacitors, a self-template route was employed to synthesize hierarchically porous NiCo_2S_4 core–shell hollow spheres. This innovative synthesis method resulted in the formation of hollow spheres with a core–shell structure, characterized by a hierarchically porous architecture. These unique structures hold promise for enhancing the performance of supercapacitors Wei et al. [16]. The core–shell hollow spheres, upon characterization, exhibited excellent long-duration cycling and a specific capacitance of 1870.2 Fg^{-1} at 2.0 Ag^{-1} . Advanced supercapacitors were developed using ultrathin nanosheets of ternary nickel cobalt iron sulfides grown on 3-D nickel nanocone arrays as binder-free electrodes. Employing a nickel plate current collector further boosted their performance [17]. This innovative technique shows promise for superior energy storage device development. Demonstrating outstanding rate capabilities, the ternary metal sulfide electrode achieved a high specific capacitance of 2159.7 Fg^{-1} at 7 Ag^{-1} . Additionally, by incorporating nickel–cobalt sulfide nanosheets, a highly compressible carbon sponge supercapacitor electrode showed significant performance enhancements [18], reaching a specific capacitance of 1093 Fg^{-1} at 0.5 Ag^{-1} in a three-electrode system. A hierarchical nickel–cobalt sulfide nanosheet array was synthesized on Ni foam via metal–organic framework derivation, enhancing electrochemical performance for supercapacitors (1406.9 Fg^{-1} at 0.5 Ag^{-1}) [19]. High-performance asymmetric supercapacitors utilized hierarchical Ni-Co-S@Ni-W-O core–shell nanosheet arrays on nickel foam, showcasing impressive specific capacitance (1988 Fg^{-1} at 2 Ag^{-1}) through hydrothermal synthesis. This innovative design and structure resulted in superior performance, making it a promising approach for high-energy storage applications [20]. Porous nickel cobalt sulfides were synthesized in a single step, with their composition tailored to enhance pseudo-capacitance performance. Among various compositions, $\text{Ni}_{1.5}\text{Co}_{1.5}\text{S}_4$ displayed the highest specific capacitance of 1093 Fg^{-1} at 1 Ag^{-1} [21]. Additionally, controllable synthesis of $\text{Ni}_{3-x}\text{Co}_x\text{S}_4$ nanotube arrays on carbon cloth substrates was achieved for high-capacity supercapacitors, with $\text{Ni}_{0.75}\text{Co}_{2.25}\text{S}_4$ exhibiting a capacitance of 1856 Fg^{-1} at 1 Ag^{-1} [22]. Sea urchin-like Ni-Co sulfides, varying in Ni to Co ratios, demonstrated superior electrochemical

performance, with $\text{Ni}_{0.25}\text{Co}_{0.75}\text{S}$ achieving a specific capacitance of 676 Cg^{-1} at 1 Ag^{-1} [23]. These findings emphasize the importance of optimizing Ni-Co ratios for tailored electrochemical properties. Furthermore, synthesizing composites of NiCo_2S_4 typically involves combining nickel (Ni), cobalt (Co), and sulfur (S) precursors with other materials to form a nanostructured composite. This approach is specifically tailored for supercapacitor applications, addressing the need for hierarchical NiCo_2S_4 structures with optimized properties. The exploration of transition metal chalcogenides (TMCs) has garnered significant attention due to their exceptional electrochemical properties, making them promising candidates for various applications such as energy storage, catalysis, and sensing. Among these, nickel cobalt sulfide (NiCo_2S_4) stands out because of its superior electrical conductivity, high electrochemical activity, and stability. The spinel structure of NiCo_2S_4 provides a unique framework that facilitates rapid electron transfer and ion diffusion, making it highly suitable for applications in supercapacitors, batteries, and electrocatalysts. Novelty of the Study, this study presents the synthesis and characterization of novel NiCo_2S_4 composites combined with advanced materials, aiming to enhance its electrochemical performance and stability. Key novelties include, innovative composite formation: integrating NiCo_2S_4 with materials like graphene oxide (GO) and carbon nanotubes (CNTs) to synergistically enhance conductivity, stability, and electrochemical performance. Optimized Synthesis Techniques: Using advanced methods such as hydrothermal, solvothermal, co-precipitation, and electrochemical deposition to identify the most efficient synthesis route. Comprehensive characterization: employing XRD, SEM, and XPS for thorough structural, morphological, and compositional analysis. Enhanced electrochemical performance: demonstrating improvements in

specific capacitance, cycling stability, and efficiency through CV, EIS, and GCD tests. Application potential: evaluating these composites in supercapacitors, batteries, and electrocatalysts to confirm their superior performance in practical applications. By addressing these aspects, this study not only advances the understanding of NiCo_2S_4 -based composites but also opens new pathways for their application in energy storage and conversion technologies. The novel synthesis strategies and detailed characterization presented here are expected to provide a solid foundation for future research and development in this rapidly evolving field.

2 Experimental details

2.1 Materials

The following high-purity chemicals were purchased from Sigma Aldrich, India: nickel nitrate hexahydrate ($\text{Ni}(\text{NO}_3)_2 \cdot 6\text{H}_2\text{O}$), cobalt(II) nitrate hexahydrate ($\text{Co}(\text{NO}_3)_2 \cdot 6\text{H}_2\text{O}$), and sodium sulfide nonahydrate ($\text{Na}_2\text{S} \cdot 9\text{H}_2\text{O}$). These chemicals were selected for their high purity and were used directly in the experimental procedures without any additional purification steps. This deliberate choice ensured the consistency and reliability of the experimental outcomes while streamlining the research process and conserving time and resources.

2.2 The hydrothermal synthesis of NiCo_2S_4 nanocomposites

Hydrothermal synthesis of NiCo_2S_4 nanocomposites was carried out following the systematic procedure described below as shown in Fig. 1. A precursor solution was prepared

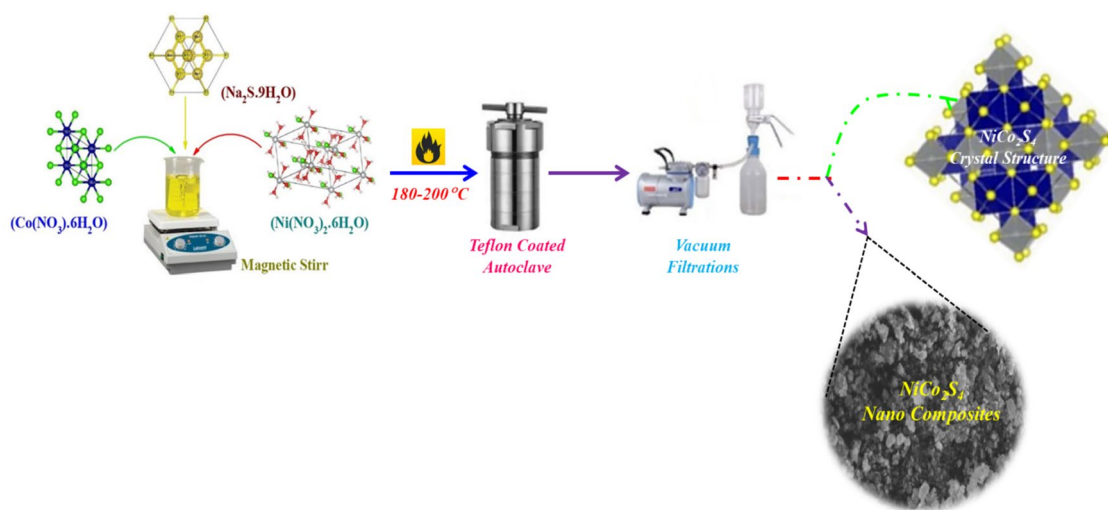
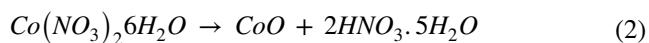
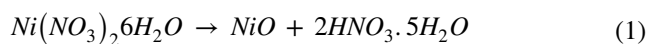
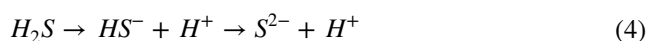


Fig. 1 Systematic procedure for the hydrothermal synthesis of a NiCo_2S_4 nanocomposite

by mixing nickel 1.3 mmol ($\text{Ni}(\text{NO}_3)_2 \cdot 6\text{H}_2\text{O}$) and 0.4 mmol $\text{Co}(\text{NO}_3)_2 \cdot 6\text{H}_2\text{O}$ in a solvent such as methanol. The molar ratios of the precursors were adjusted according to the desired composition of the nanocomposite. A sulfur source such as ($\text{Na}_2\text{S} \cdot 9\text{H}_2\text{O}$) was added to the precursor solution and the amount of sulfur source was carefully controlled to achieve the desired stoichiometry. To control the pH of the solution, pH adjustment was considered important for the formation and stability of the nanocomposite by adding a base such as potassium hydroxide (KOH) or ammonium hydroxide (NH_4OH). To ensure homogeneity, the solution was thoroughly dispersed using magnetic stirring to facilitate nanocomposite formation. The prepared solution was transferred to a suitable reaction vessel such as a Teflon-lined autoclave and the reaction vessel was placed in a high-pressure autoclave and subjected to hydrothermal conditions. For this study, the reaction was conducted at a precise temperature of 180 °C for 24 h. This specific temperature and time were chosen to achieve the desired flower-like morphology and optimal electrochemical properties of the Ni-Co-S nanostructures on the Ni mesh substrates. This was followed by removal of residual impurities such as ethanol or water, and the resulting nanocomposite was rinsed thoroughly with a suitable solvent and filtered. Finally, the nanocomposite was collected and dried thoroughly under vacuum or at controlled temperature. During the reaction, the sulfur atoms from the sulfur source replace the oxygen atoms from the metal nitrates, resulting in the formation of metal sulfides. The exact mechanism and intermediate species involved in the formation of NiCo_2S_4 can be complex and may depend on factors such as temperature, precursor concentrations, reaction time, and the presence of additional additives or surfactants. It is important to note that detailed studies and experimental investigations are often conducted to further understand the precise reaction pathway, intermediates, and mechanisms involved in the formation of NiCo_2S_4 using specific synthesis conditions.



During this process, the Ni^{2+} and Co^{2+} ions engage in reactions with the S^{2-} ions existing in the Na_2S anionic solution. The possible reactions that may take place are depicted as follows,



When Na_2S dissolves in an aqueous solution, it generates S^{2-} ions. These ions undergo hydrolysis, leading to the creation of HS^- and H_2S species. These species serve as sulphur sources for the ion-exchange reaction, aiding in the transformation of Ni and Co precursors to produce NiCo_2S_4 .

2.3 Electrochemical analysis

The setup of the two-electrode system is depicted in Scheme as shown in Fig. 2. The working-electrode power (WE power) and working-electrode sensing (WE sense) leads from the electrochemical workstation were connected to one side of the anode electrode, while the reference electrode (RE) and counter electrode (CE) leads from the electrochemical workstation were connected to the other side of the cathode electrode. In this arrangement, two identical or different composite electrodes were fully enclosed within filter paper soaked with 6 M KOH an electrolyte. The filter paper served dual roles: it absorbed and retained the electrolyte necessary for the electrochemical reaction of the two-electrode system, and it acted as a separator between the two composite electrodes. The electrochemical performance was assessed using a CHI600E series workstation at St. Joseph's College (Autonomous), Tiruchirappalli. This evaluation included cyclic voltammetry (CV), galvanostatic charge/discharge, and electrochemical impedance measurements. During CV assessments, a cyclic potential sweep was initiated from an initial voltage of -0.4 V and concluded at a final voltage of 0.6 V. Galvanostatic charge/discharge (GCD) tests were conducted to assess the energy storage capabilities of the electrode material. Electrochemical impedance (EIS) measurements were carried out across a frequency range from 1 Hz to 100 kHz, using an AC amplitude of 10 mV and a bias potential of 0.4 V.

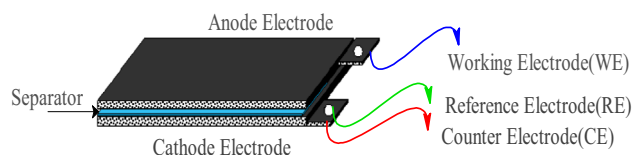


Fig. 2 A scheme and an image of two-electrode configuration

2.4 Supercapacitor anode and cathode electrode fabrication method

Supercapacitors are devices that efficiently store and release energy by utilizing two electrodes, namely a positive electrode and a negative electrode, which are separated by an electrolyte. The fabrication process of these electrodes involves the use of various materials. These materials include a carbon-based substance such as Graphene Oxide (GO) or reduced Graphene Oxide (rGO), a conductive binder such as polyvinylidene fluoride (PVDF) or polytetrafluoroethylene (PTFE), a conductive additive like activated carbon black, a solvent such as N-methyl-2-pyrrolidone (NMP), and a substrate such as stainless-steel plate. To create the anode electrode, a mixture of materials is prepared. This mixture consists of graphene oxide powder (10 wt.%), an active metal oxide powder material called NiCo₂S₄ nanocomposite (80 wt.%), conductive additive GO, binder polytetrafluoroethylene (PTFE) (10 wt.%), and N-methyl-2-pyrrolidone solvent. The desired ratios of these materials are thoroughly mixed. The same procedure is repeated to fabricate the cathode electrode, but with a different electrode material mixture. This mixture involves blending 90 wt.% of active graphene oxide powder, 10 wt.% of binder polytetrafluoroethylene (PTFE), and the appropriate amount of N-methyl-2-pyrrolidone solvent. To manufacture the electrodes, the substrate, such as stainless-steel plate, is first cut into the desired size and shape, typically 1 cm x 1 cm, the active mass 3 mg cm⁻². Next, the electrode slurry is applied onto the substrate using either a doctor's blade or a spin coater. Afterward, the coated substrate is dried in an oven set at 80 °C for several hours, allowing the solvent to evaporate and leaving behind the electrode material securely attached to the substrate.

2.5 Fabrication of NiCo₂S₄ ASC devices

The electrodes for the supercapacitor are prepared using specific materials. The positive electrode is constructed using a composite called NiCo₂S₄, while the negative electrode is made of GO (Graphene Oxide). To fabricate the ASC (Asymmetric Supercapacitor) devices, these electrodes are assembled along with a separator soaked in a 6 M KOH electrolyte solution. The assembly is completed by connecting the electrodes with a copper wire. Once the ASC devices are fabricated, their electrochemical performance is evaluated using several characterization techniques. These techniques include cyclic voltammetry (CV), which measures the current response as a function of voltage, galvanostatic charge–discharge (GCD), which evaluates the energy storage and release capability, and electrochemical impedance spectroscopy (EIS), which analyzes the impedance behavior of the device. These characterization methods provide

valuable insights into the performance and behavior of the ASC devices.

2.6 Electrode connections in a three-electrode system

In electrochemical systems in Fig. 2, particularly in supercapacitors or any cell using a three-electrode configuration, the terms "anode" and "cathode" can be misleading compared to their use in batteries. In such systems, the working electrode (WE) is typically where electrochemical reactions occur, such as ion adsorption or desorption on materials like activated carbon or metal oxides. This electrode is connected to the anode of the potentiostat or galvanostat, allowing precise control of the potential or current during tests.

The reference electrode (RE) provides a stable, known potential against which the working electrode's potential is measured. It is connected to the cathode of the potentiostat or galvanostat, ensuring accurate measurement and control of the potential difference during experiments like cyclic voltammetry (CV) or galvanostatic charge–discharge (GCD). The counter electrode (CE) completes the circuit and facilitates current flow during measurements. It is also connected to the cathode of the potentiostat or galvanostat, ensuring smooth current flow between the working electrode (anode) and counter electrode (cathode) through the electrolyte, maintaining electrochemical equilibrium for accurate measurements. Connecting the working electrode to the anode and the reference and counter electrodes to the cathode of the potentiostat or galvanostat in a three-electrode system ensures proper control and measurement of electrochemical processes. This setup is crucial for accurately assessing performance parameters such as specific capacitance, energy density, and cycle stability of supercapacitor materials.

2.7 Characterization techniques

Several characterization techniques can be employed to analyze the properties of NiCo₂S₄ materials. Here are the commonly used techniques for characterization: Bruker, FT-IR spectroscopy (and the ALPHA II) is utilized to analyze the functional groups and chemical bonds present in the NiCo₂S₄ material. It provides information about the molecular vibrations and can help identify the presence of specific bonds or compounds. X-ray diffraction (XRD) analysis of NiCo₂S₄ materials can be conducted utilizing the Rigaku Ultima III diffractometer. This instrument operates at 40 kV and 40 mA and utilizes Cu K α radiation (wavelength of 1.54 Å) as the X-ray source. X-ray photoelectron spectroscopy (XPS) can be employed to investigate the chemical states of the elements. Field emission scanning electron microscope (Zeiss Sigma model: FEI quanta 250) are used to

analyze the surface and morphological behavior of NiCo₂S₄ composite. The existences of elements like Ni, Co and S have been determined by energy dispersive X-ray analysis (EDX). The electrochemical performance was assessed using a CHI600E series. This evaluation included cyclic voltammetry (CV), galvanostatic charge/discharge, and electrochemical impedance measurements.

3 Results and discussion

3.1 X-ray diffraction (XRD) analysis of NiCo₂S₄

Figure 3 displays the XRD patterns of NiCo₂S₄ nanocomposite prepared. NiCo₂S₄ is a ternary compound consisting of nickel (Ni), cobalt (Co), and sulfur (S). It belongs to the spinel crystal structure, which is a type of cubic crystal system. Within the spinel structure, the metallic cations (Ni and Co) are situated in octahedral and tetrahedral sites, whereas the sulfur ions occupy the remaining tetrahedral sites. The expected XRD pattern for NiCo₂S₄ will exhibit characteristic diffraction peaks corresponding to the crystal structure. These peaks can be indexed using the Miller indices and can be used to determine lattice parameters and crystallographic information. Typically, the XRD pattern for NiCo₂S₄ will show diffraction peaks at specific angles (2θ) corresponding to the following Miller indices. The XRD peaks at approximately 17°, 27°, 31.8°, 38.68°, 47°, 52°, 56°, 59°, 65°, and 70° can be assigned to the (111), (220), (311), (400), (500), (502), (440), (622), (533), and (444). The crystal planes of nickel cobalt sulfide containing metallic elements. (NiCo₂S₄), each in its respective location. In sampling NiCo₂S₄ nanocomposite, an apex was detected. at 31.8°, which aligns with the Ni-Co-S composition materials,

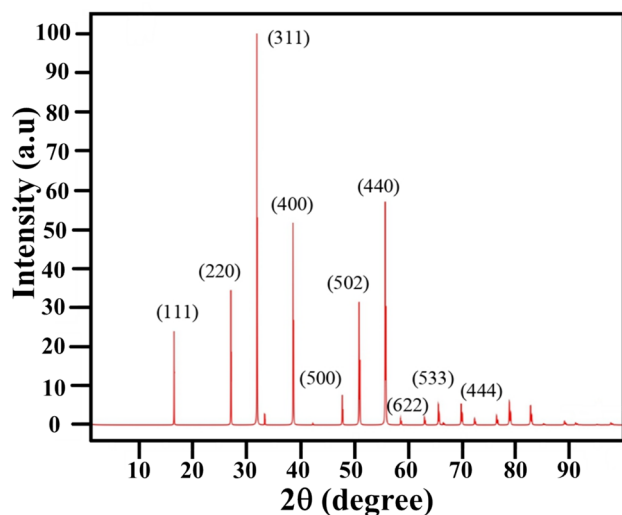


Fig. 3 XRD pattern of the NiCo₂S₄ Nano Composites

as depicted in Fig. 3 [24]. Additionally, a prominent peak at 38.68° was observed, originating from the Ni foam. The positions and intensities of all the peaks closely correspond to those listed in the JCPDS card 020–0782, suggesting that the synthesized composites exhibit a cubic crystal structure with lattice parameters, $a = b = c = 9.32531$, $\alpha = \beta = \gamma = 90^\circ$ and Unit-cell volume = 810.941015 Å [25]. Furthermore, the crystalline size of NiCo₂S₄ is determined using Scherrer equation given as follows $D = K\lambda/\beta\cos\theta$, where K represents Scherer's constant and β is the full width at half maximum intensity of the dominant peak. The calculated crystallite size of NiCo₂S₄ is 38.45 nm [26]. These results align well with standard findings. Consequently, it can be inferred that the successful formation of NiCo₂S₄ nanocomposite has been achieved [27].

3.2 X-ray photoelectron spectroscopy (XPS) analysis of NiCo₂S₄

The core level spectra depicted in Figs. 4a–d focus on the specific energy levels associated with Ni-2p, Co-2p, and S-2p orbitals. The peaks observed at 850.40 eV and 878.44 eV in the Ni 2p spectrum can be attributed to the Ni -2p_{3/2} and Ni -2p_{1/2} states, respectively. Similarly, the peaks at 788.22 eV and 801.35 eV in the Co -2p spectrum correspond to the Co -2p_{3/2} and Co -2p_{1/2} states. These results provide evidence for the presence of Ni and Co in the nanocomposite. Furthermore, the disparity in energy between the Ni -2p and Co -2p peaks, which is measured to be 17.50 and 15.67 eV, respectively, indicates variations in the valence states of Ni and Co. The values suggest the presence of Ni²⁺, Ni³⁺, Co²⁺, and Co³⁺ ions within the nanocomposite, reflecting different oxidation states of the elements [28]. Within the core level spectra of S- 2p, the peak identified at 166.55 eV aligns with the S- 2p_{1/2} state. This provides evidence for the presence of sulfur (S²⁻) in the NiCo₂S₄ nanocomposite. Overall, The XPS examination verifies the composition of the NiCo₂S₄ nanocomposite, highlighting the presence of Ni²⁺, Co²⁺, Ni³⁺, Co³⁺, and S²⁻ ions. These findings are consistent with previously reported data, indicating the reliability and validity of the experimental results [29].

3.3 Raman spectrum analysis of NiCo₂S₄

Raman spectroscopy is a technique used to analyze the vibrational modes of molecules based on their scattering of laser light as shown in Fig. 5. NiCo₂S₄ is a compound known as nickel cobalt sulfide (Ni-Co-S), and its Raman spectrum provides valuable information about its molecular structure and vibrational modes. Raman spectroscopy is a technique that analyzes the interaction of light with molecular vibrations, producing a characteristic spectrum based on the energy shifts observed in the scattered light.

Fig. 4 a XPS spectrum of the optimized NiCo₂S₄ Nano composites b–d Core level spectra for Ni 2p, Co 2p, and S 2p Nano composites

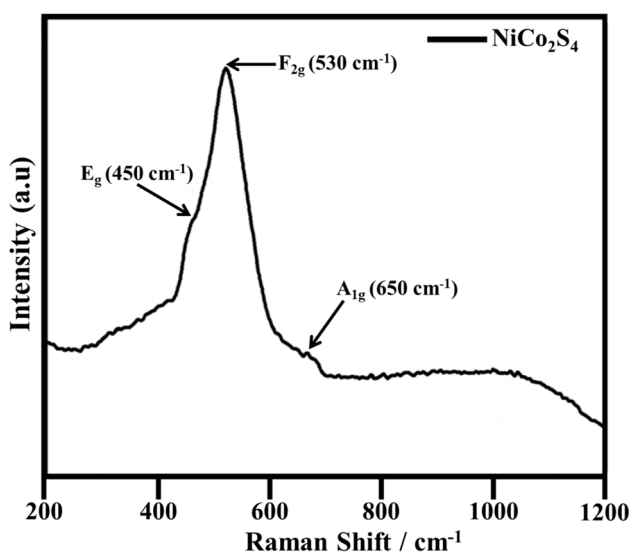
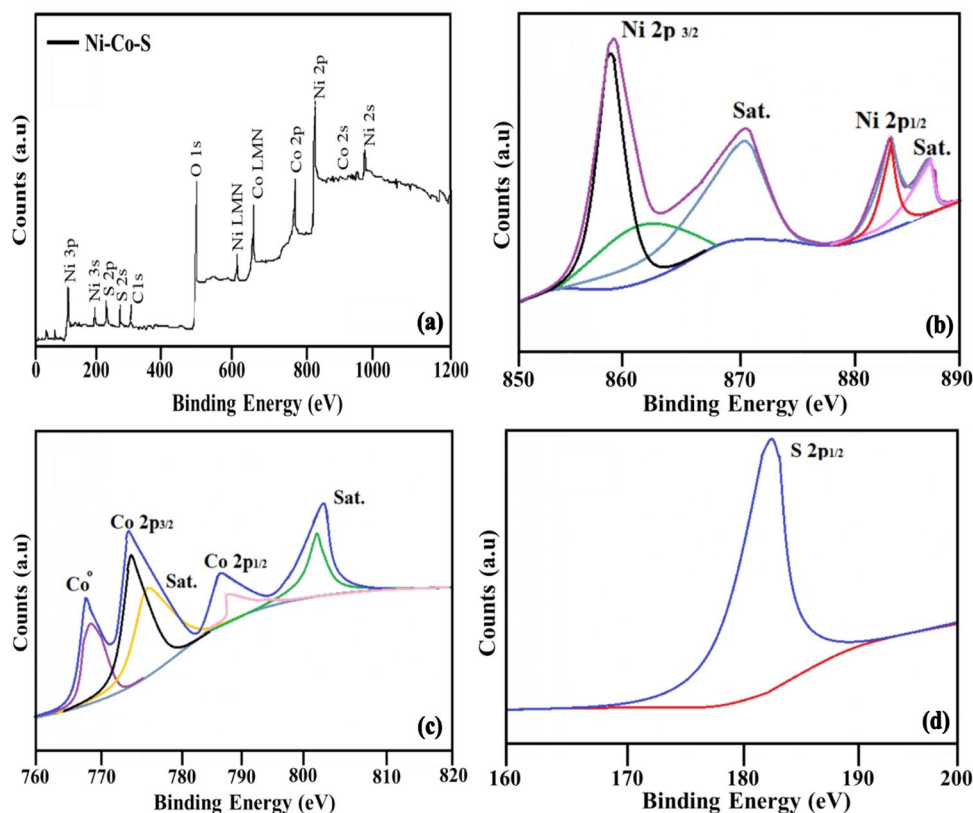


Fig. 5 Raman spectrum of the NiCo₂S₄ Nano composites

In the Raman spectrum of NiCo₂S₄, various vibrational modes can be identified, indicating the specific vibrational and rotational motions of atoms within the compound. The Raman peaks can be attributed to the vibrations of sulfur (S) and metal (Ni and Co) atoms present in the structure. The Raman spectrum of NiCo₂S₄ typically exhibits several prominent peaks, including: *Low-frequency region (below*

400 cm⁻¹): A peak around 120 cm⁻¹ corresponds to the stretching vibration of metal-sulfur (M-S) bonds. Peaks in the range of 180–250 cm⁻¹ arise from the torsional modes of the M-S bonds and sulfur ring vibrations. *Intermediate-frequency region (400–800 cm⁻¹):* Multiple peaks in this region correspond to the stretching and bending vibrations of sulfur atoms. Peaks around 450 cm⁻¹ and 530 cm⁻¹ arise from sulfur breathing modes, involving the in-plane and out-of-plane vibrations of sulfur atoms. The peak around 620 cm⁻¹ corresponds to the symmetric stretching mode of the sulfur atoms. *High-frequency region (above 800 cm⁻¹):* Peaks around 820 cm⁻¹ and 940 cm⁻¹ are attributed to the stretching vibrations of metal–oxygen (M–O) bonds. A peak around 1,030 cm⁻¹ corresponds to the symmetric stretching mode of sulfur atoms. Additional peaks in this region may arise from other molecular vibrations and lattice effects [30].

3.4 FT-IR spectrum analysis of NiCo₂S₄

In general, the FT-IR spectrum of NiCo₂S₄, which is a ternary metal sulfide compound as shown in Fig. 6, is expected to exhibit several characteristic absorption bands associated with metal–oxygen and metal-sulfur vibrations. Here are some potential peak positions and their corresponding vibrational modes. The stretching vibrations of metal–oxygen bonds typically occur in the higher frequency region of the spectrum, ranging from approximately 3620 cm⁻¹.

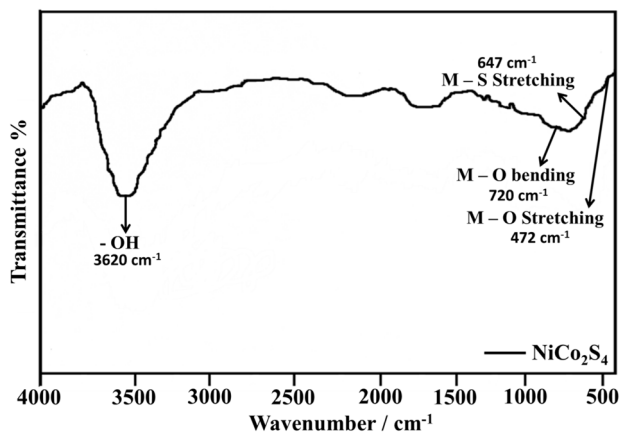


Fig. 6 FT-IR spectrum of the NiCo₂S₄ Nano composites

Bending vibrations involving metal–oxygen bonds are usually observed in the mid-frequency region, around 720 cm⁻¹. Stretching vibrations of metal-sulfur bonds generally appear in the mid-frequency region, around 647 cm⁻¹. Stretching vibrations involving metal- oxygen bonds often occur in the lower frequency region, ranging approximately 472 cm⁻¹ [31].

3.5 FE-SEM and EDX analysis of NiCo₂S₄

The field-emission scanning electron microscopy (FE-SEM) images of the NiCo₂S₄nanocomposite. Figures 7a–b exhibited micrometer and nanometer sized grains of NiCo₂S₄nanocomposite. Field-emission scanning electron microscopy is a powerful imaging technique used to

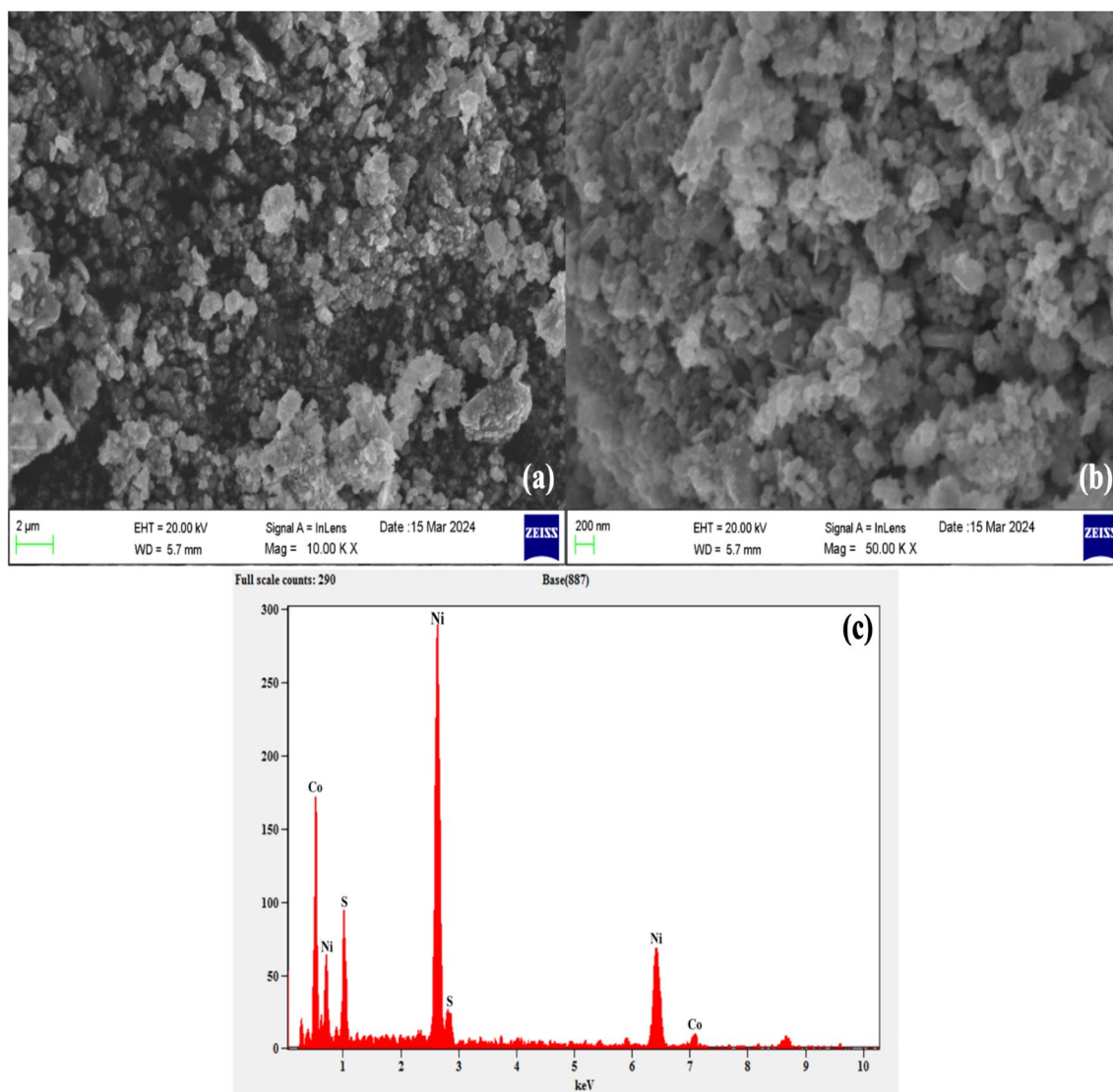


Fig. 7 FE-SEM images of the NiCo₂S₄ Nano composites with different magnification **a** 2 μm **b** 200 nm and **c** EDX spectrum of NiCo₂S₄ Nano composites

examine the surface morphology of materials at high and lower magnifications. In the case of NiCo_2S_4 , FE-SEM analysis can reveal the morphology of the material, such as the shape and size of the particles or crystalline structures. It can also provide information about the distribution and arrangement of these particles [32]. *Spherical stone nanoparticles*: NiCo_2S_4 nanocomposites can also contain spherical stone nanoparticles observed in lower magnification. These nanoparticles are generally characterized by a uniform size and shape, appearing as distinct, rounded particles in the FE-SEM images. The dimensions of these nanoparticles may fluctuate based on the synthesis technique and parameters. *Interconnected Spherical stone*: NiCo_2S_4 nanocomposites higher magnification may exhibit interconnected Spherical stone like structure. These interconnected spherical stone have a thin and flat morphology with irregular edges. In the FE-SEM images, these interconnected spherical stones NPs would appear as a network or mesh-like structure, where individual spherical stones are connected to each other [33, 34]. A higher porous surface area in the NiCo_2S_4 nanocomposite can be advantageous for several reasons. Here are a few key points to consider: *Enhanced reactivity*: The presence of a higher porous surface area provides a larger active surface for reactions to occur. This can be beneficial for various applications, such as catalysis or energy storage, as it allows for increased contact between the nanocomposite and the reactants or electrolytes, leading to enhanced reaction rates and improved performance. *Increased adsorption capacity*: The porous structure of the nanocomposite offers more available sites for the adsorption of molecules or ions. This is particularly useful in applications such as gas adsorption, where a higher porous surface area can lead to improved gas storage or separation capabilities. *Efficient mass transport*: The porous network facilitates the transport of reactants, products, or ions within the nanocomposite. The interconnected pores allow for easier diffusion of species, reducing mass transport limitations and improving overall reaction efficiency. *Electrochemical performance*: In energy storage devices like batteries or supercapacitors, a higher porous surface area enables more accessible electroactive sites, promoting faster charge transfer and higher energy storage capacity.

Additionally, the porous structure can accommodate the volume changes that occur during charge–discharge cycles, enhancing the stability and cyclability of the nanocomposite. Attaining enhanced electroconductivity in the C nanocomposite can have several advantages for various electronic and energy-related applications. Here are a few key points to consider: *Improved charge transport*: A higher electrical conductivity facilitates the movement of charge carriers within the nanocomposite. This is particularly important in electronic devices, such as sensors, transistors, or conductive coatings, where efficient charge transport is essential for

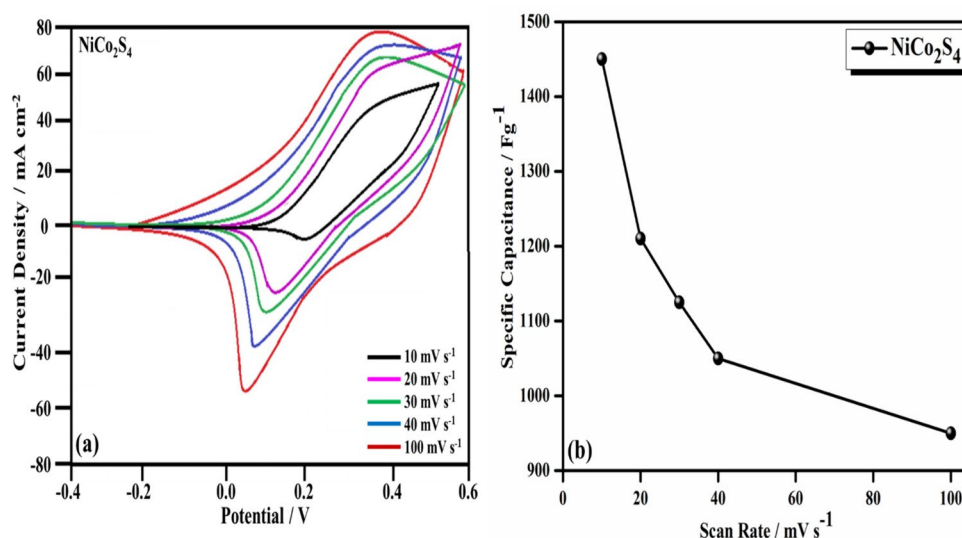
optimal performance. *Enhanced energy storage*: In energy storage devices, such as batteries or supercapacitors, a higher electroconductivity enables faster charge/discharge rates and lower internal resistance. This leads to improved power density and energy efficiency. *Better catalytic activity*: In catalytic scenarios, improved electrical conductance can bolster the efficiency of charge transfer mechanisms occurring at the interface between the catalyst and electrolyte. This improves the overall catalytic efficiency, making the nanocomposite more effective in various electrochemical processes, like oxygen reduction reactions (ORR) or hydrogen evolution reaction (HER). *Reduced resistive losses*: Higher electrical conductivity minimizes resistive losses in the nanocomposite, reducing energy dissipation and improving overall energy conversion efficiency. This is particularly crucial in applications like energy harvesting or power electronics. The EDX analysis investigates the composition of the NiCo_2S_4 structure. The characteristic EDX spectrum of such has shown the presence of Ni, Co and S as illustrated in Fig. 7c. The obtained percentage of such elements is near its theoretical atomic percentage. The non-existence of other elements ensures the phase – pure NiCo_2S_4 composites structures as explained in the XPS analysis [35, 36].

3.6 Electrochemical analysis of NiCo_2S_4

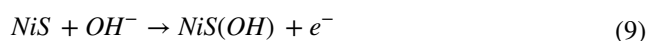
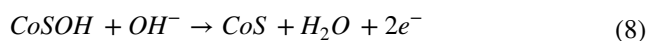
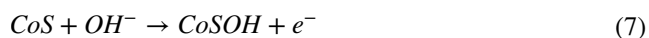
3.6.1 Cyclic voltammetry (CV) analysis of NiCo_2S_4

In this study, we explored the cyclic voltametric (CV) technique behavior of the NiCo_2S_4 nanocomposite with equal molar Ni and Co ratios. Figure 8a display the CV curves obtained at various scan rates ranging from 10 to 100 mV s^{-1} . The measurements were conducted using a 6 M KOH electrolyte to provide a suitable environment for electrochemical reactions. As shown in Fig. 8a, two distinct redox peaks are observed in all CV curves of the NiCo_2S_4 composite. These peaks are indicative of the pseudocapacitive behavior and faradaic reactions associated with the composite material. The existence of two redox peaks indicates the likelihood of reversible Faradaic reactions within the NiCo_2S_4 nanocomposite [37]. These reactions involve the reversible interconversion of oxidation states of the nickel and cobalt cations, adding to the collective charge storage capability of the material. The pseudo capacitance observed in the CV curves indicates additional capacitive behavior resulting from surface absorption and release processes at the electrode–electrolyte boundary. The position and shape of the redox peaks remain consistent across the different scan rates investigated. This suggests that the electrode kinetics and charge transfer processes within the NiCo_2S_4 nanocomposite are relatively independent of the scan rate [38]. However, the peak currents vary with the scan rate, with higher currents observed at faster scan rates due to

Fig. 8 **a** C-V Curves NiCo₂S₄ electrode at different scan rates **b** The specific capacitance of the NiCo₂S₄ nanocomposite



increased charging and discharging rates. The appearance of two redox features in the cyclic voltammogram (CV) curves of the NiCo₂S₄ nanocomposite demonstrates its ability to store charges through both pseudocapacitive and faradaic mechanisms [39, 40]. This dual contribution enhances the overall energy storage capacity and performance of the material, making it suitable for supercapacitor applications. The NiCo₂S₄ nanocomposite displayed the highest peak intensity in the redox reaction attributed to the varied oxidation states of Ni²⁺ and Co²⁺ in the KOH electrolyte. These oxidation states significantly influenced the distinct peaks observed in the electrochemical behavior of the nanocomposite.



Effect of Scan Rate: At lower scan rates (10 mV s⁻¹), the cyclic voltammogram exhibits well-defined redox peaks, suggesting efficient charge storage and fast redox reactions. As the scan rate increases, the peak currents become broader and lower in magnitude. This behavior indicates that higher scan rates impose kinetic limitations on the charge transfer processes, leading to decreased capacitive behavior. Furthermore, at higher scan rates (100 mV s⁻¹), the redox peaks tend to merge and become less distinguishable. This phenomenon suggests the occurrence of diffusion-limited behavior, where the ions cannot effectively access the electrode surface and participate in the redox reactions within the limited time frame provided by the faster scan rate [41]. Comparing our results with previous studies, the scan rate dependence of NiCo₂S₄ shows similarities with other transition metal

sulfides, indicating common electrochemical characteristics. However, it is worth noting that NiCo₂S₄ exhibits a distinctive redox behavior due to its unique structural and compositional features, which may result in enhanced charge storage capabilities. **Specific Capacitance Analysis:** The specific capacitance values of the NiCo₂S₄ electrode were determined by integrating the area under the relevant cyclic voltammograms using the following equation:

$$C_s = \frac{1}{mv(V_c - V_a)} \int_{V_a}^{V_c} I(V) dV \quad (10)$$

The specific capacitance (C_s) can be determined by integrating the area under the relevant cyclic voltammetry (CV) curves using the following the above specific capacitance equation, where C_s is the specific capacitance (Fg⁻¹), the active mass of the electrode material was maintained at 3 mg/cm². This specific mass loading ensures adequate active material on the electrode for electrochemical testing, providing reliable and consistent performance metrics for the Ni-Co-S nanostructures synthesized on the Ni mesh substrates. The potential difference ($V_c - V_a$) represents the voltage range, and v denotes the scanning speed or scan rate. The specific capacitance values showed a decreasing trend as the scan rate increased. Specifically, the specific capacitance values were found to be 1450 Fg⁻¹, 1210 Fg⁻¹, 1125 Fg⁻¹, 1050 Fg⁻¹, and 950 Fg⁻¹ for scan rates of 10 mV s⁻¹, 20 mV s⁻¹, 30 mV s⁻¹, 40 mV s⁻¹, and 100 mV s⁻¹, respectively. Figure 8b presents the specific capacitance values of NiCo₂S₄ at different scan rates. The specific capacitance decreases with increasing scan rate, indicating a strong dependence on the rate at which the potential is scanned. This behavior can be attributed to several factors, including the reduced time available for ion diffusion and the limited

accessibility of active sites at higher scan rates. These limitations hinder the effective utilization of the electrochemically active surface area, resulting in reduced specific capacitance values. Although the specific capacitance decreases with increasing scan rate, indicating reduced charge storage capacity, NiCo₂S₄ still exhibits promising electrochemical performance. Its unique structural properties, including the presence of both nickel and cobalt cations, contribute to its favorable redox behavior and capacitive characteristics [42].

3.6.2 Galvanostatic charge–discharge (GCD) analysis

The galvanostatic charge–discharge (GCD) curves of the NiCo₂S₄ nanocomposite at a current density of 10 mA cm⁻² in a 6 M KOH electrolyte can be organized as follows. To determine the suitable operational voltage range for supercapacitors, it is essential to consider the stability of the electrolyte and electrode materials. For example, in aqueous electrolytes like 1 M KOH, the operational voltage typically ranges from 0 to 1.2 V. Setting up the supercapacitor cell involves a three-electrode configuration: the working electrode (WE) is connected to the anode of the potentiostat/galvanostat, the reference electrode (RE) is connected to the cathode of the potentiostat/galvanostat, and the counter electrode (CE) is also connected to the cathode of the potentiostat/galvanostat. Proper immersion of electrodes in the electrolyte solution, such as 1 M KOH, ensures efficient ion transport during measurements. The GCD curves, shown in Fig. 9a represent the charge and discharge behavior of the NiCo₂S₄ nanocomposite. During the charge process, the potential gradually increases as the electrode absorbs ions from the electrolyte and stores energy. On the discharge process, the potential decreases as the stored energy are released. The specific capacitance of the NiCo₂S₄ nanocomposite was calculated using the following equation.

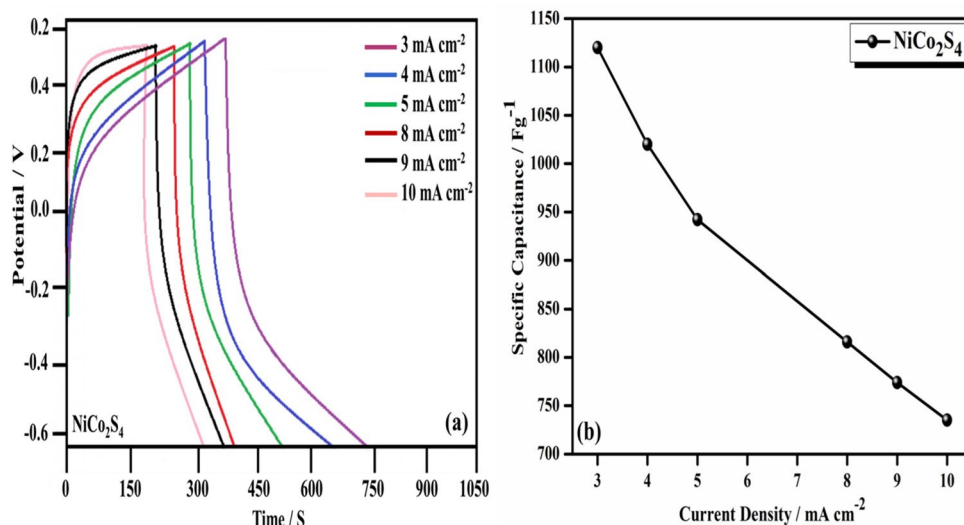
$$\text{Specific capacitance } (C_{\text{specific}}) = \frac{I \times \Delta t}{m \times \Delta V} \quad (11)$$

Where I is the applied current density, Δt is the discharge time, m is the mass of the active material, and ΔV is the potential window. *Interpretation of Results:* The charge–discharge curves reveal certain characteristics of the NiCo₂S₄ nanocomposite. One notable feature is the absence of distinct plateaus, indicating the absence of a purely pseudocapacitive behavior. Instead, the curves show a smooth slope, suggesting a combination of both double-layer capacitance and pseudocapacitive contributions [43]. The charge–discharge curves of the NiCo₂S₄ electrode were plotted in Fig. 9a, depicting its behavior at various current densities ranging from 3 to 10 mA cm⁻² in a 6 M KOH electrolyte. Subsequently, the specific capacitance of the NiCo₂S₄ electrode was determined and observed to be 1120, 1020, 942, 816, 774, and 735 Fg⁻¹ at current densities of 3, 4, 5, 8, 9, and 10 mA/cm², respectively. These specific capacitance values are illustrated in Fig. 9b. In conclusion, the galvanostatic charge–discharge curves and specific capacitance values provide insights into the electrochemical behavior and energy storage capability of the NiCo₂S₄ nanocomposite. The combination of double-layer capacitance and pseudocapacitance contributes to its overall performance [44]. A Ragone plot illustrates the trade-off between energy density and power density, providing insights into the overall performance of the supercapacitor. Energy density (E) is calculated using the formula:

$$E = \frac{1}{2} C_s (\Delta V)^2$$

where C_s is the specific capacitance and ΔV is the voltage range. Power density (P) is calculated using formula:

Fig. 9 a Charge–Discharge curves of NiCo₂S₄ at a current density of 10 mA cm⁻² b GCD specific capacitance of the NiCo₂S₄ nanocomposite



$$P = \frac{E}{\Delta t}$$

where Δt is the discharge time. Voltage stability and GCD curves are monitored periodically to detect any changes in charge storage behavior. Evaluating supercapacitors using GCD curves, Ragone plots, and cycle stability studies provides comprehensive insights into their electrochemical performance. These analyses help optimize electrode materials, electrolyte compositions, and device architectures to enhance energy storage efficiency and cycle life, making them suitable for practical applications in energy storage systems, portable electronics, and electric vehicles [45].

3.7 Electrochemical impedance spectroscopy analysis

Electrochemical impedance spectroscopy (EIS) was employed to analyze the electrical characteristics of NiCo_2S_4 samples that were prepared with equimolar Ni/Co ratios. The obtained results are presented in Fig. 10, showcasing the Nyquist plots corresponding to the NiCo_2S_4 electrodes. The analysis of the NiCo_2S_4 nanocomposite using electrochemical impedance spectroscopy (EIS) yielded several important parameters that can provide insights into its electrical properties. The obtained results and their corresponding discussions are presented below: *Nyquist Plot*: The Nyquist plot of the NiCo_2S_4 nanocomposite electrodes displayed a semicircular arc in the high-frequency region followed by a linear tail at lower frequencies. This observation suggests the presence of both charge transfer and diffusion processes in the electrochemical reactions of the nanocomposite. *Electrochemical Impedance*: The impedance magnitude ($|Z|$) and phase angle (θ) were measured at different frequencies [46].

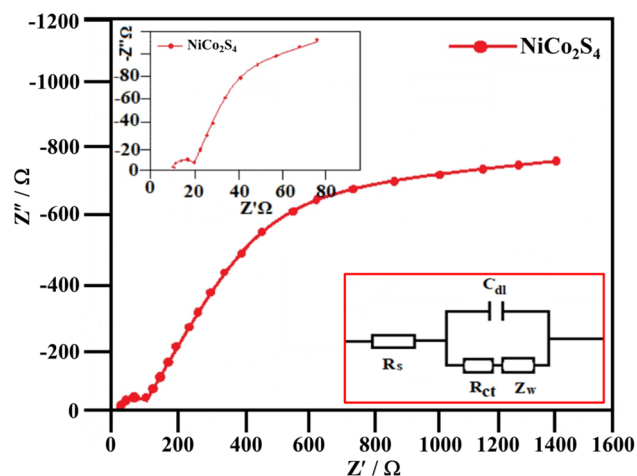


Fig. 10 Nyquist plots obtained for the NiCo_2S_4 nanocomposite electrodes in a 6 M KOH electrolyte with equivalent circuit for EIS fitting

The impedance magnitude indicates the overall resistance to charge transfer processes, while the phase angle reveals the relationship between the applied voltage and the resulting current phase shift. *Charge Transfer Resistance (R_{ct})*: The charge transfer resistance (R_{ct}) was determined by analyzing the semicircular arc in the Nyquist plot. A higher R_{ct} value suggests a slower charge transfer process, indicating a larger resistance to electron transfer at the electrode–electrolyte interface. *Double-Layer Capacitance (C_{dl})*: The double-layer capacitance (C_{dl}) was calculated based on the linear portion of the Nyquist plot at lower frequencies. C_{dl} symbolizes the electrochemical double layer established at the interface between the electrode and electrolyte, and provides information about the surface area and charge storage capability of the nanocomposite. *Warburg Impedance (Z_w)*: The linear tail observed at lower frequencies in the Nyquist plot corresponds to the Warburg impedance (Z_w). Z_w is associated with the diffusion of species within the electrode material and provides insights into the ion diffusion processes in the nanocomposite [47]. The EIS analysis of the NiCo_2S_4 nanocomposite revealed valuable information about its electrical properties. The presence of a semicircular arc in the Nyquist plot indicates the combination of charge transfer and diffusion processes in the electrochemical reactions of the nanocomposite. The higher value of charge transfer resistance (R_{ct}) suggests a slower charge transfer kinetics, possibly due to the presence of surface defects or a limited active surface area. The calculation of double-layer capacitance (C_{dl}) provides insights into the surface area and charge storage capability of the nanocomposite. A higher C_{dl} value indicates an increased surface area, which is beneficial for electrochemical processes and energy retention purposes. The linear tail observed at lower frequencies corresponds to the Warburg impedance (Z_w), reflecting the diffusion processes within the nanocomposite [48]. The analysis of Z_w can provide information about the ion diffusion rates and the accessibility of the electrode material for charge transport. The electrical properties of the NiCo_2S_4 nanocomposite samples were evaluated, encompassing parameters such as solution resistance (R_s), charge transfer resistance (R_{ct}), Warburg impedance (Z_w), and double-layer capacitance (C_{dl}). The measured values for R_s were 15.4 Ω , and the R_{ct} value was determined as 83.2 Ω for the NiCo_2S_4 samples, respectively. The EIS fitted parameters were calculated and listed in Table 1.

Table 1 Electrochemical Impedance Spectroscopy Parameters.

Double layer capacitance (C_{dl})	Charge transfer resistance (R_{ct})	Warburg impedance (Z_w)	Constant phase element (CPE)
10.5 mF cm^{-2}	1.2 Ω	45 Ω	7.8 mF cm^{-2}

The recorded data on solution resistance reveal that the NiCo₂S₄ composite displayed decreased charge transfer resistance. These findings imply that the NiCo₂S₄ composite showcased reduced solution and charge transfer impedances, likely due to its elevated electrical conductivity and highly porous nanostructured NiCo₂S₄ composites. The presence of a semicircular curve in the Nyquist plot obtained from electrochemical impedance spectroscopy (EIS) is indicative of a combination of charge transfer and diffusion processes occurring in the electrochemical reactions of the nanocomposite. In the diagram, the semicircular pattern illustrates the impedance reaction of the system across varying frequencies. The center of the semicircle, known as the capacitive loop, corresponds to the charge transfer process at the electrode–electrolyte interface [49]. The low charge transfer resistance and high double layer capacitance indicate excellent electrochemical performance, while the Warburg impedance suggests efficient ion diffusion. Together, these characteristics contribute to the superior performance of the synthesized material in energy storage applications.

3.7.1 Understanding operational voltage and safe potential window for supercapacitors using aqueous electrolytes

In the context of supercapacitors, especially those using aqueous electrolytes like 1 M KOH, the operational voltage for the anode and cathode, and the safe potential window are critical considerations to ensure device performance and longevity. For the anode (working electrode), the operational voltage typically ranges from 0 V to 1.2 V vs. the reference electrode (Ag/AgCl or SCE). The anode may be charged up to 1.2 V and discharged down to 0 V during cyclic voltammetry (CV) or galvanostatic charge–discharge (GCD) tests. The cathode (reference electrode), connected to the reference electrode in a three-electrode setup, typically operates at a negative potential relative to the reference electrode. In aqueous electrolytes like 1 M KOH, the operational voltage for the cathode can range from about –1.2 V to 0 V vs. the reference electrode. The cathode may be charged up to 0 V and discharged down to –1.2 V during electrochemical measurements [50].

The safe potential window refers to the range of voltages within which the supercapacitor can operate reliably without risking degradation or damage to its electrodes and electrolyte. For aqueous electrolytes like 1 M KOH, the safe potential window for the anode ranges from 0 V to 1.2 V vs. the reference electrode, while for the cathode, it ranges from –1.2 V to 0 V vs. the reference electrode. Consequently, the safe operational potential window for the entire supercapacitor device spans from –1.2 V (cathode limit) to 1.2 V (anode limit) vs. the reference electrode.

For practical applications, maintaining stable voltage operation within the specified potential window is essential to avoid electrolyte decomposition and electrode degradation. Selecting electrode materials that can withstand the applied voltages without undergoing irreversible reactions or structural changes is crucial. Additionally, ensuring that the chosen electrolyte is stable within the operational potential window helps prevent side reactions and maintain long-term device performance. Understanding the operational voltage for the anode and cathode, along with the safe potential window for the entire supercapacitor device, is crucial for designing and optimizing electrochemical performance. These parameters guide the selection of materials and electrolytes, ensuring reliable operation and longevity in various applications such as energy storage systems, portable electronics, and electric vehicles.

This process involves the transfer of electrons between the electrode surface and the electrolyte solution. The radius of the semicircular curve in the Nyquist plot is influenced by the charge transfer resistance (R_{ct}). A greater R_{ct} value implies a deceleration in charge transfer kinetics, indicating that the pace of electron transfer between the electrode and the electrolyte is comparatively sluggish. This can be attributed to factors such as surface passivation, surface roughness, or limited active surface area of the nanocomposite. Slower charge transfer kinetics can have implications for the performance of the nanocomposite in various electrochemical applications. It may affect the efficiency of energy storage or conversion processes, as well as the overall electrochemical reaction rate. Strategies to reduce R_{ct} , such as optimizing the electrode material or modifying the surface properties, can be explored to enhance the charge transfer kinetics and improve the electrochemical performance of the nanocomposite [51]. In addition, comparative specific capacitance of the NiCo₂S₄ Nano composites and other earlier reports summarized in Table 2.

4 Conclusion

To summarize, we accomplished the successful synthesis of a nanocomposite resembling NiCo₂S₄ using the hydrothermal method. The specific capacitance findings revealed that NiCo₂S₄ displayed enhanced performance due to its compact morphology. Nevertheless, the interconnected nanoflake structure of NiCo₂S₄ yielded the highest specific capacitance, reaching 1450 Fg⁻¹ at 10 mV s⁻¹. Consequently, we have effectively devised a fresh approach for constructing the architecture of the NiCo₂S₄ nanocomposite, showcasing its potential as a highly promising material for supercapacitor applications.

Table 2 Comparative Specific Capacitance of the NiCo₂S₄ and other earlier reports

S. No	Positive electrode	Negative electrode	Current density	Electrolyte	Operational voltage	Specific capacitance (F g ⁻¹)	References
1	NiCo ₂ S ₄ @CNT	Carbon cloth	0.5 A g ⁻¹	polyvinyl alcohol/KOH gel as solid electrolyte	0–1.3	1,123 F g ⁻¹	44
2	NiCo ₂ S ₄ @mesocarbon microbead (NCS@MCMB) composite	Active carbon (AC)	1 A g ⁻¹	3 M KOH aqueous	0–1.4	936 F g ⁻¹	45
3	NiCo ₂ S ₄ (FSNCS)	Active carbon (AC)	1 A g ⁻¹	1 M KOH aqueous	0–1.5	559.3 F g ⁻¹	46
4	NiCo ₂ S ₄	Porous carbon (PC)	1 A g ⁻¹	2 mol L ⁻¹ KOH aqueous solution	0–6	1350 F g ⁻¹	47
5	MXene/NiCo ₂ S ₄		1 A g ⁻¹		0–0.5	1211.1 F g ⁻¹	48
6	NiCo ₂ S ₄ (NCS) nanosheet on SiO ₂ @C core-shell nanospheres (SiO ₂ @C-NCS nano-composite)	Carbon nanotube paper	1 mA cm ⁻²	KOH		625 F g ⁻¹	49
7	NiCo ₂ S ₄	GO	2 mA cm ⁻²	6MKOH	0–3	1450 F g ⁻¹	This work

Author contributions A.Premkumar contributed to writing of the original draft, validation, investigation, methodology and writing of the original draft. B.Sridevi contributed to supervision, investigation, writing, review and editing. K.S.Mohan contributed to validation, writing of the original draft, review and editing.

Funding The authors declare that no funds, grants, or other support were received during the preparation of this manuscript.

Data availability My manuscript has no associated data.

Declarations

Competing interests On behalf of all authors, the corresponding author states that there is no conflict of interest.

Ethical approval The local Institutional Review Board deemed the study exempt from review.

References

- Jiang Y, Qian X, Zhu C, Liu H, Hou L (2018) ACS Appl Mater Interfaces 10:9379–9389
- Chen W, Xia C, Alshareef HN (2014) ACS Nano 8:9531–9541
- Zhang C (2018) Adv Sci 5:1700375
- Ahuja P, Ujjain SK, Kanojia R (2018) Appl Surf Sci 427:102–111
- Ujjain SK, Sahu V, Sharma RK, Singh G (2015) Electrochim Acta 157:245–251
- Rajesh JA (2018) J Ind Eng Chem 63:73–83
- Pu J (2014) ChemPlusChem 79:577–583
- Xiao T et al (2018) Electrochim Acta 269:397–404
- Chen H et al (2013) Highly conductive NiCo₂S₄ urchin-like nanostructures for high-rate pseudocapacitors. Nanoscale 5:8879–8883
- Li X, Li Q, Wu Y, Rui M, Zeng H (2015) ACS Appl Mater Interfaces 7:19316–19323
- Shen L et al (2015) Nat Commun 6:6694
- Tie J et al (2018) J Mater Sci Mater Electron 29:2251–2258
- Wang T et al (2015) J Mater Chem A 3:23035–23041
- Zhang G (2013) & (David) Lou. X W Sci Rep 3:1470
- Xiao J, Zeng X, Chen W, Xiao F, Wang S (2013) Chem Commun 49:11734–11736
- Wei C et al (2018) Appl Surf Sci 453:288–296
- Rahimi S, Shahrokhian S, Hosseini H (2018) J Electroanal Chem 810:78–85
- Liu Q, Jin J, Zhang J (2013) ACS Appl Mater Interfaces 5:5002–5008
- Liang X et al (2018) ACS Appl Mater Interfaces 10:10087–10095
- Tao K, Han X, Ma Q, Han L (2018) Dalt Trans 47:3496–3502
- He W et al (2018) Nano Res 11:1415–1425
- Ding R, Gao H, Zhang M, Zhang J, Zhang X (2015) RSC Adv 5:48631–48637
- Saad Goma M, Iftikhar H (2018) Jae-Jin. Shim, Nanoscale 10:6620–6628
- Panneerselvam A, Mohan KS, Marnadu R et al (2022) J Sol-Gel Sci Technol 102(597):613
- Sui Y et al (2018) Adv Mater Interfaces 5:1800018
- Wei X et al (2017) Chem Electro Chem 4:2634–2642
- Mohan KS, Panneerselvam A, Marnadu R, Chandrasekaran J, Shkir M, Tataroğlu A (2021) Inorg Chem Commun 129:108646
- Wei W et al (2014) Chem Mater 26:3418–3426
- Pu J et al (2014) ACS Sustain Chem Eng 2:809–815
- Yang X et al (2018) ChemElectroChem 5:1576–1585
- Mohan KS, Marnadu R, Shin Y, Gunavathy KV, Balasubramani V, Ubaidullah M, Shkir M, Reddy VRM, Kim WK (2023) Surf Interfaces 39:102887
- Khoo SY et al (2015) Adv Mater Interfaces 2:1500384
- Shinde SK, Dubal DP, Ghodake GS, Kim DY, Fulari VJ (2014) J Electroanal Chem 732:80–85
- Xiao J, Wan L, Yang S, Xiao F, Wang S (2014) Nano Lett 14:831–838
- Shen L et al (2015) Adv Energy Mater 5:1400977
- Mohan KS, Panneerselvam A, Chandrasekaran J, Marnadu R (2021) Shkir Mohd. Appl Nanosci 11:1617–1635
- Shinde SK, Ghodake GS, Fulari VJ, Kim D-Y (2017) J Ind Eng Chem 52:12–17
- Chou S-W, Lin J-Y (2013) J Electrochem Soc 160:D178–D182

39. Chen Y-Y, Dhaiveegan P, Michalska M, Lin J-Y (2018) *Electrochim Acta* 274:208–216
40. Chen W, Fan Z, Gu L, Bao X, Wang C (2010) *Chem Commun* 46:3905–3907
41. Chen JS, Guan C, Gui Y, Blackwood DJ (2017) *ACS Appl Mater Interfaces* 9:496–504
42. Luan Y, Zhang H, Yang F, Yan J, Zhu K, Ye K, Wang G, Cheng K, Cao D (2018) *Appl Surface Sci* 447:165–172
43. Minghai Yao X, Ji XO, Peng W, Cheng S (2022) *J Power Sources* 543:231829
44. Gao Y, Lin Q, Zhong G, Yanbao Fu, Ma X (2017) *J Alloy Compd* 704:70–78. <https://doi.org/10.1016/j.jallcom.2017.01.304>
45. Akkinepally B, Nadar NR, Reddy IN, Rao HJ, Nisar KS, Shim J (2024) *J Alloys Compd* 970:172677
46. Zhang Y, Zhang Y, Zhang Y et al (2019) *Nano-Micro Lett* 11:35. <https://doi.org/10.1007/s40820-019-0265-1>
47. Wang J, Wang J, Zhu G, Huarui X, Zhang X, Zhao Y, Zhang J, Jiang K, Aibing Yu (2022) *J Energy Storage* 46:103907
48. Li X, Fu Y, Ma H et al (2020) *J Chem Sci* 132:101. <https://doi.org/10.1007/s12039-020-01806-0>
49. Qi J, Gu H, Ruan C et al (2022) *Ionics* 28:2979–2989. <https://doi.org/10.1007/s11581-022-04516-4>
50. Harisha BS, Akkinepally B, Shim J, Lim J (2024) *J Energy Storage* 87:111466
51. Sajjad U, Jiang Y, Linlin Guan X, Chen AI, Zhang S, Ren Y, Zhou X, Liu Z (2020). *Nanotechnol.* <https://doi.org/10.1088/1361-6528/ab4d0a>

Publisher's Note Springer Nature remains neutral with regard to jurisdictional claims in published maps and institutional affiliations.

Springer Nature or its licensor (e.g. a society or other partner) holds exclusive rights to this article under a publishing agreement with the author(s) or other rightsholder(s); author self-archiving of the accepted manuscript version of this article is solely governed by the terms of such publishing agreement and applicable law.

Authors and Affiliations

A. Premkumar¹ · B. Sridevi¹ · K. S. Mohan²

✉ A. Premkumar
rennieprem@gmail.com

K. S. Mohan
mohanm.scm.phil@gmail.com

¹ PG and Research Department of Chemistry, Presidency College, Chennai, Tamil Nadu 600 005, India

² Department of Physics, Nandha Engineering College (Autonomous), Erode, Tamil Nadu 638 052, India